Received 4 January 2024; revised 31 January 2024; accepted 11 February 2024. Date of publication 14 February 2024; date of current version 26 March 2024.

Digital Object Identifier 10.1109/OJAP.2024.3366070

Optimization and Evaluation of a 3-D Ray Tracing Channel Predictor Individually for Each Propagation Effect

MICHAEL SCHWEINS[1], LENNART THIELECKE[1], NILS GRUPE[1,2], AND THOMAS KÜRNER[1] (Fellow, IEEE)

[1]Institute for Communications Technology, Technische Universität Braunschweig, 38106 Braunschweig, Germany

[2]HMF Smart Solutions GmbH, 31848 Bad Münder, Germany

CORRESPONDING AUTHOR: M. SCHWEINS (e-mail: m.schweins@tu-braunschweig.de)

This work was supported in part by the German Federal Ministry for Digital and Transport (BMDV) under Grant VB5GFWOTUB; in part by the Open Access Publication Funds of Technische Universität Braunschweig; and in part by the Framework of COST Action CA20120 IRACON.

ABSTRACT For 5G/6G system simulations and radio planning the availability of both accurate and run-time efficient channel predictors is required. This paper presents a 3D ray tracing channel predictor, which takes into account the relevant propagation phenomena like free space propagation, reflection, scattering, diffraction and transmission. The predictor is validated by two types of measurements and the relevance of the various propagation phenomena is analyzed based on predictions in a city using real base station locations and building data. Based on these results an acceleration methodology for the search of reflected paths is derived, which is able to reduce the computation time to 40% compared to the baseline prediction.

INDEX TERMS 5G, beamforming, channel prediction, pathloss, ray tracer, SiMoNe.

I. INTRODUCTION

THE FAST growing use of today's mobile communication spawned the fifth generation (5G) and enabled research on the sixth generation (6G). Both generation places higher technical demands for sophisticated radio planning. Urban 5G networks are intended to utilize spectrum at 3.6 GHz or even 26 GHz which requires a much denser network than currently deployed. In order to provide target coverage and exploit the scarce radio frequency spectrum the development of more accurate and reliable prediction methods gets into the focus.

Common statistical approaches provide computationally inexpensive predictions based on empirical data derived through intensive measurement campaigns. They offer a fast approach for generating predictions and require significantly less input parameters [1], [2]. However, the abstraction and therefore generalization of the environment lacks in precision for uncommon or special scenarios [3]. To investigate mobile radio channels in wireless networks more accurately, location specific channel models must be used for predictions [4]. Especially when considering highly directive antennas, e.g., based on beamforming techniques, only deterministic prediction methods like ray tracing or ray launching are able to resolve dedicated Multi-Path-Components (MPCs). Those MPCs exhibit individual angles with respect to the corresponding Transmitter (TX) or Receiver (RX) position, required for correct consideration of highly directive antenna patterns. Also Intelligent Reflecting Surfaces (IRSs) or Relay Surfaces introduce new challenges predicting the radio channel due to their strongly angular dependent behavior. For given incident and emitted patterns of these special surfaces, a ray tracer is able to consider such devices precisely in the prediction.

A ray tracer takes into account a wide range of input parameters. Its prediction accuracy highly depends on the existence and level of detail of the input data (e.g., 3D building data, material parameters, vegetation, weather data). Though, the algorithms usually suffer from a high computation time for big input vectors.

Various acceleration techniques for ray tracing algorithms are introduced in the literature, either programmatically or methodically [10], [11]. Hardware-oriented programming languages, parallelization or special hardware like GPUs can increase the performance of the algorithms enormously [12]. Furthermore, there are also approaches to suspend the search for MPCs above a certain distance, which is another source of significant run-time savings. The authors of [13] propose a threshold distance of 500 m for radio predictions at 1.8 GHz, derived from intensive measurements. Another approach is to specialize the algorithms for individual application scenarios. Assuming that in a Vehicle-to-Vehicle (V2V) scenario all buildings are higher than the TX and RX antennas, a two-dimensional view of the scenario is sufficient. In [14] this approach was exploited to pre-compute visibility checks between surfaces, allowing it to perform channel prediction in near real-time.

The ray tracer presented in this paper is designed to predict the radio channel generically for various types of scenarios and is valid for a wide range of frequency. E.g., in [15], the ray tracer is applied for 300 GHz and [14] introduces a modified but derived version of it at 5.9 GHz. However, these publications relate to fundamentally different simulation scenarios, the description of the used algorithms is lacking of detail and the evaluation methodology is restricted to qualitative metrics of the prediction. In this paper our scenario focus is on the classical mobile radio topology with a cell site several meters above the roof tops. The common frequency band for this topology lies between 700 MHz and 3.8 GHz. The ray tracer contains several acceleration methods from which only a few are scenario-dependent which will be described in the next section. The special feature of the introduced ray tracer is that the individual propagation effects can be considered, validated and post-processed individually and separately from each other. Up to now this ray tracing algorithms were not presented in this accuracy.

The contribution of this paper is threefold:

- Introduction and validation of the ray tracer based on a publicly available and generally agreed dataset
- Application to new frequency bands and other scenario characteristics
- Analysis of various propagation effects in a cellular network scenario and derivation of a corresponding acceleration technique

The second Section of this paper introduces the in-house developed ray tracing algorithms and its input data. Several acceleration methods are introduced and discussed. A validation with an open source data set is presented in Section III. The ray tracing algorithms are evaluated in the fourth Section based on mobile radio measurements performed in an urban area. We then take a closer look into a ray tracing prediction result for coverage maps in Section V to identify characteristics with respect to cell site location and the surrounding buildings. An acceleration technique for the search of reflected rays is derived from this investigation and discussed with regard to its benefits and impact to prediction quality. Finally, the paper is concluded in Section VI.

II. RAY TRACER FEMTOPRED

The algorithms of the 3D ray tracing channel predictor are part of the Simulator For Mobile Networks (SiMoNe) [8]. This multi-level simulation suite, developed and maintained at the Technische Universität Braunschweig, includes and combines channel predictions, link level simulations [9] and system level simulations. This software framework allows on the one hand for storing large datasets in a well designed and modular structure inside a database, on the other hand to work with this data utilizing sophisticated algorithms [7]. The so called FemtoPred is one of SiMoNes' radio channel predictors. Its parameters enable to use either stochastic models like Okumura Hata, deterministic models for ray tracing or a combination of both where a threshold distance can be set to switch between the models. However, this work only investigates FemtoPreds' ray tracing part, in which deterministic models for all individual propagation effect are implemented, i.e., reflection, transmission, scattering and diffraction.

Required input data for FemtoPreds' ray tracing predictions are

- 3D building data
- material parameters represented by the permittivity to calculate the interactions' effect of the electromagnetic wave with the matter
- TX and RX characteristics like
  - location
  - transmit power
  - frequency
  - antenna diagrams, direction and tilt

Building data consists of multiple plane surfaces, which are polygon shaped areas within a 2D plane. Those can be freely oriented inside the 3D environment. Surfaces could for instance be housing walls in city scenarios or tiny structure details for small scenarios like rooms. It is worth noting that next to static buildings moving obstacles like cars, buses, etc. could be treated as a source of reflection, diffraction and obstruction as well. Each surface contains properties like thickness, roughness, orientation and material. These surface parameters in combination with frequency specific material parameters indicate the alteration of the electromagnetic wave when it hits the surface. Material parameters are measured and published for many materials on a frequency-specific basis, e.g., [16], [17], [18].

Antenna diagrams account for radiation pattern and the directive gain of the antennas. In order to derive a power prediction from the channel prediction, all MPCs are weighted with the antennas radiation pattern according to their angle of arrival (AOA) and angle of departure (AOD), respectively, and multiplied with TX transmission power. Due to reciprocity, it does not matter whether the antenna is transmitting or receiving [6]. According to

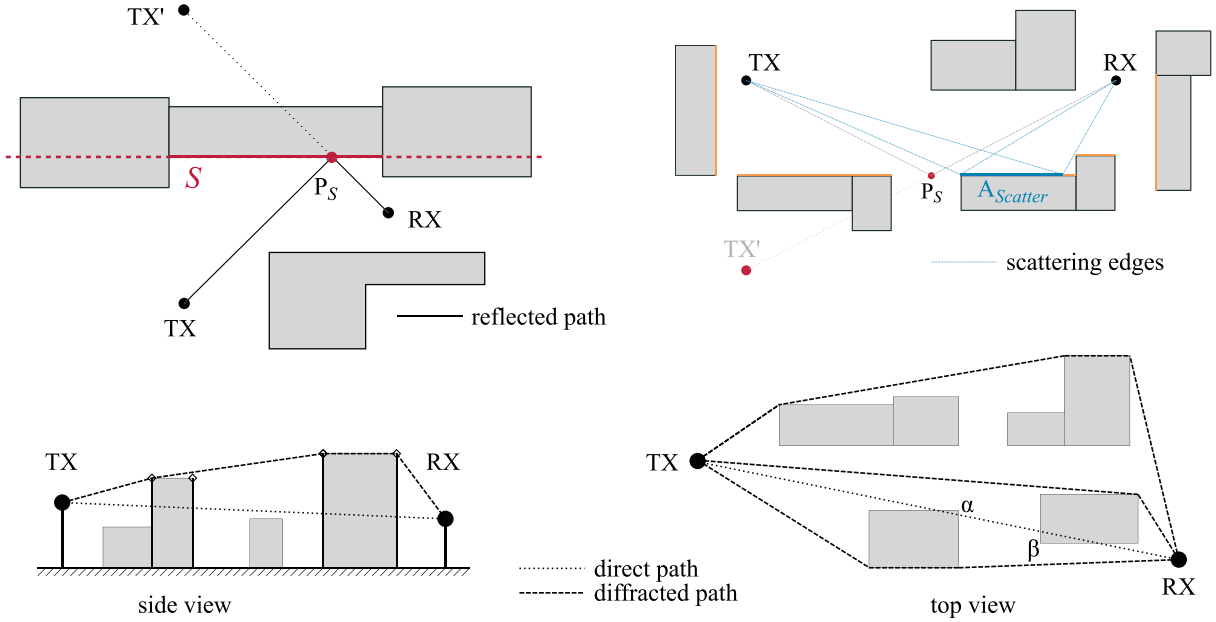

FIGURE 1. Propagation effects for rays within a scenario. Top left shows a reflected ray on surface S at point P_S. Top right illustrates a scenario with a scattering surface $A_{Scatter}$. A reflecting path is not valid since P_S is not on a surface. Bottom left visualize a side view on a scenario. The buildings assemble a height profile from which a path with horizontal diffraction is derived. Bottom right shows a scenario with vertically diffracted rays between TX and RX.

this, received power prediction in FemtoPred is a two-step process: First, it calculates so called isotropic channel predictions without consideration of any antenna diagrams. They could be applied in a second step, which allows for more flexibility due to separation of the tasks. Crucial to the correct application of the antenna patterns is not only the precise TX and RX antenna position, but also their azimuth alignment and tilt, both mechanically and electrically.

When performing pathloss predictions the FemtoPred firstly searches valid paths between TX and RX. Afterwards complex attenuations are calculated for valid paths, which indicate the modification of an electromagnetic wave on this particular path. The following paragraphs briefly introduce the FemtoPreds' methods for determining valid paths.

Rays can propagate between two points in a scenario with different effects. The most obvious path is a unobstructed direct ray between TX an RX in a Line-Of-Sight (LOS) scenario. The free space pathloss equation specifies the attenuation and phase shift of the ray [5]. Propagating energy may also interact with surfaces, leading to reflected, transmitted or diffracted propagation paths. Non-specular reflections from surfaces result in scattered paths.

Reflection: SiMoNe's FemtoPred determines reflected paths using the image source method. For first order reflections at surface S, first the point TX is mirrored at the plane of S, resulting in the mirror point TX' (see Fig. 1, top left). If the straight line $\overline{\text{TX'RX}}$ crosses the surface S, a possible reflection point P_S is found. Finally, the lines of sight from TX to P_S and from P_S to RX have to be evaluated. If there is no blockage by other surfaces, an unobstructed reflected ray from TX via the interaction point P_S to RX is found.

For the prediction Pair TX-RX, the search for reflected rays must be performed for each surface in the scenario to determine all possible reflected paths. To search for second-order reflections, i.e., with two reflecting interaction points, the re-mirroring of the first-order image sources is required at all surfaces. Thus, the computational cost increases exponentially with reflection order n since the number of image sources i follows

$$i = k \cdot (k-1)^{n-1}.$$

The amount of surfaces k in the scenario therefore has also a significant impact on the required computational power.

To calculate the attenuation and phase shift due to the interaction, different methods are implemented in SiMoNe. As the simplest method, material parameters without any angular dependency can be utilized which might cause inaccurate results. More correctly as a second method, the Fresnel Equations predict the differing behavior of waves that are incident upon a material interface. The Transfer-Matrix Method (TMM) extends this model to solve scenarios with surfaces that exhibit stratified materials, like a wall with dedicated thickness [20], [21].

Scattering: According to Snell's law, the angle of incidence at surface S of a reflected ray equals the angle of reflection. This is often stated as 'specular reflection' at location P_S. If the interaction point P_S does not lie on the surface S, this surface, although possibly being located in the field of view of both TX and RX, does not contribute any specular reflected energy in the modeling, see for example Fig. 1 (top right). Especially for rough surfaces, the phenomenon of non-specular reflection has a non-negligible influence, which is why FemtoPred also determines so-called

scattered rays. The algorithm divides the surfaces into sub-surfaces with a pre-defined area and checks whether these sub-surfaces are in the field of view of both TX and RX. If this is the case, these scattered rays contribute to non-specular reflected energy from TX to RX. Depending on the size of the sub-surface and the total number of surfaces, the search for scattered rays can increase the computational effort tremendously and may make the simulation infeasible. The FemtoPred utilizes the Modified Equivalent Current Approximation (MECA) method to determine the attenuation and phase shift of scattered rays [22].

Diffraction: Reflection and scattering take place onto surfaces, which are derived from static building data or moving obstacles. In contrast, edge points of these surfaces can lead to diffracted paths, which can run over building roofs on the one hand (horizontal diffraction) or around building corners on the other hand (vertical diffraction). In principle, a distinction can be made between vertical and horizontal diffraction and also the complexity in ray tracing for these two phenomena differs greatly. For roof diffraction, i.e., horizontal diffraction, first the direct link between TX and RX is determined to identify all surfaces intersected by this direct path. The height of these surfaces then gives the elevation profile, from which the path of the roof diffraction is derived. Fig. 1 (bottom left) shows the LOS path between TX and RX is shown as a thin dotted line. The heights of the intersected lines, visualized as diamonds, span the diffraction profile that forms the resulting path, shown as dashed line. Applying the commonly used multiple knife edge diffraction with the Deygout model [5] gives the attenuation of the corresponding ray.

The vertical, or side diffraction is much more complex to determine, because not only the visibility between the corner points is decisive. Due to the Deygout model their orientation and the course of the ray needs to be considered. Thus, seen from a bird's eye view, a beam cannot be bent once clockwise around a corner and then counterclockwise. The direction of rotation must remain the same. The bottom right plot of Fig. 1 represents an exemplary scenario with three bent beams drawn as dashed lines. The upper beam exhibit three edges, the middle and the bottom beam one and two edges, respectively. A path across the corners α and β is not valid, because the direction of diffracted energy changes as described above. From the course of the vertically diffracted beam, a 2D diffraction profile can be derived, with which the attenuation of the beam can be calculated by applying the Deygout model [19].

Transmission: Transmission represents another possible type of propagation where the path passes through blocking surfaces from TX to RX. The TMM takes into account the finite thickness of the irradiated material and thus gives phase-correct complex attenuation [20].

SiMoNes' FemtoPred combines models for direct, reflected, scattered, diffracted and transmitted wave propagation. Each possible path is stored in a so called ray-object, which contains information about the complex attenuation, the interaction points (e.g., point where the reflection takes place on a surface) and AOD and AOA. Those angles enable to consider antenna gain as a function of AOA and AOD. To determine the path loss between two points, all predicted rays between these points are first masked with the antenna pattern and then summed up complexly. The Received Signal Strength (RSS) then results from

$$\mathrm{RSS} = \mathrm{P_{TX}} \cdot \left| \sum_{i=0}^{N_{\mathrm{MPC}}} \frac{\mathrm{G}(\mathrm{AoD}_i)}{\overline{\mathrm{PL}_i}} \right| \tag{1}$$

with the transmit Power of TX $\mathrm{P_{TX}}$, the antenna gain G depending on the MPC's AOD and the complex path loss $\overline{\mathrm{PL}}$.

How the TX and RX points are determined depends on the cell and/or device location inside the simulation scenario. The FemtoPred offers different prediction modes (Cell-to-Device, Cell-to-Cell, Cell-to-Map (C2M) and Device-to-Device) which determine how TX-RX-pairs are generated. An additional filtering of prediction pairs is possible allowing for individual scenario setups.

For Map-predictions, the scenario is rasterized into a rectangular, evenly sized grid of variable grid size. Each of those n_{Map} Pixels form a so called prediction pair with each n_{Cells} Cell. Therefore the FemtoPred has to predict all $n_{\mathrm{Map}} \cdot n_{\mathrm{Cells}}$ prediction pairs.

Acceleration methods for Ray Tracing: Since ray tracing in large scenarios with lots of surfaces can lead to long computation time, the FemtoPred includes different types of acceleration methods. Some of them are applicable for ray tracing in general, others only for special prediction modes.

In 1980, Rubin and Whitted could show that the search for blocking obstacles (surface intersections) can significantly be accelerated by first checking the 3D bounding box of the corresponding building for any intersection [23]. This reduces the number of intersections for each building to six, no matter how many surfaces are included in the building. Only if the ray hits the six-sided bounding box, the FemtoPred performs a complete computation of all surface intersections. However, reducing the scenarios complexity by preprocessing building data is a common technique as well [24]. Merging nearby surfaces or deleting fine structures decreases the number of surfaces inside the scenario but has to be done in consideration of losing details.

In SiMoNe each surface exhibits a well defined front and a back side. That enables filtering of possible interaction effects individually for front and back sides. For example if only outdoor positions are considered as RX inside a map based prediction, channel degradation due to transmission into a building then reflection inside this building and finally transmission out of the building could be assumed to be negligible. Therefore, interaction effects on the back side of surfaces could be limited to transmission. A significant acceleration gain can be reached by considering only relevant

buildings with respect to the type of ray and the purpose of the prediction. Far away buildings can be neglected, e.g., validating the LOS path does not require to consider buildings located behind or next to RX (seen from TX). [24] and [25] propose Fresnel zones with TX and RX positions as focal points to filter out relevant surfaces. With the ellipsoid method a maximum expected path length of a first order reflected ray is considered, ignoring all reflecting surfaces that would lead to greater path lengths. Next to the filtering with Fresnel zones, FemtoPred offers the possibility to filter buildings of rectangular zones with an R-tree [26]. Due to the structure, this search tree offers great speed ups for filtering spatial data as applied in ray tracing scenarios. These acceleration methods can lead to a small degradation of path loss prediction accuracy, depending on the choice of filter parameters such as ellipse size or R-tree bounding box size. When predicting other channel parameters such as delay spread, this acceleration approach is not suitable without further elaboration to avoid missing any details.

As mentioned in the previous section, the complexity of searching for reflection paths increases exponentially with the maximum order of reflection. With increasing reflection order, though, the power contribution of a path decreases, which is why the FemtoPred allows for a dynamic reduction of the reflection order depending on the order of previously found rays. For example, in case a first-order reflection path was found for a TX-RX pair the FemtoPred could skip search for reflection paths with an order of three or higher.

To determine vertical diffraction, edges need to be identified. In general, an edge is spanned by two adjacent surfaces, but only outbound edges are valid diffraction edges. Identifying such and adding the information about it to the building data accelerates the FemtoPred significantly. From a diffraction order of two, it is also worthwhile to determine and store all other visible diffraction edges for each edge.

For Cell-to-X predictions the FemtoPred could take advantage of the static TX position. The search for possible Image Sources for potential reflecting points or diffraction edges from the TX perspective keeps constant for different RX positions. Therefore the FemtoPred offers the possibility to perform a pre-calculation step to identify those static points for each TX position. The search for reflected paths then consists only of the LOS-check between the pre-calculated Image Source positions and RX. For example, a 10 km × 10 km city scenario with a grid size of 5 m results in 4 million RX-pixels. Determining the TX Image Source positions once in advance leads to a huge speed up. However, depending on the number of TXs and surfaces inside the scenario but especially also the maximum reflection order, the memory required for the Image Source positions may exceed the available RAM size of the PC, which is why sequential prediction may be necessary for the individual TX positions.

TABLE 1. Performance of FemtoPreds' path loss prediction with two configurations for the three routes individually and on average.

	Route1		Route2		Route3		average
Con-fig.	STD [dB]	mean [dB]	STD [dB]	mean [dB]	STD [dB]	mean [dB]	STD [dB]
#1	7.9	-13.1	6.3	-10.3	8.5	-9.3	8.1
#2	7.4	-1.2	6.5	1.8	7.7	1.3	7.5

III. VALIDATION OF RAY TRACING PATHLOSS PREDICTIONS

In order to validate SiMoNes' FemtoPred algorithms its prediction results were compared with measurements published in COST231 [28]. A pathloss measurement campaign has been carried out in downtown Munich by the German GSM network operator Mannesmann Mobilfunk GmbH. It is performed at 947 MHz, the TX and RX height is 13 m and 1.5 m above ground, respectively. Next to the 2356 measurement points of the three measurement routes (total length of about 25 km), building data in vector format covering an area of about 2.4 km × 3.4 km in downtown Munich have been provided [27]. Table 1 summarizes the prediction performance of the FemtoPred. Configuration #1 indicates the prediction results of the FemtoPred with the models as described in the literature without any parameter calibration. The material of the buildings is assumed to be concrete and the dielectric parameters are taken from [16]. Rays are searched for a maximum reflection order of 3, diffraction over roofs and side walls, scattering and transmission. Configuration #2 describes the same setup but with parameter adjustments. As described in [28], 11 randomly chosen measurement points were utilized for calibration purpose. This results in a material parameter for the buildings of $\epsilon_r = 6$ and $\epsilon_i = -12$ and a power offset of -12.5 dB.

Differences between pathloss measurement and prediction may be due to the inaccuracies of the building data and prediction models but also due to disregarding of further details like cars, roofs, balconies and vegetation effects. Since the transmitting antenna height is below roof-top of most of the buildings within the scenario, almost all RX locations are in Non-LOS situations.

The authors in [28] introduce several pathloss prediction algorithms which are also validated with the COST231 data set. Most of them achieve an average standard deviation of about 7 dB up to 9 dB. Also newer publications validate their introduced path loss prediction algorithms and acceleration techniques with the Mannesmann Munich dataset [29], [30], [31], [32]. The standard deviation of these models is similarly within the above-mentioned value range. Since the prediction accuracy of the FemtoPred is also within this range, a sufficient prediction quality of the algorithms can be assumed.

The computing time for the Munich dataset validation varies between 3.47 s in [29] and 120 s in [30]. However, in some cases the computing time is not stated at all (all

models presented in [28]) or it remains unclear whether pre-processing is included. Also the utilized hardware differs greatly. The FemtoPred takes 0.6 s for pre-processing and 7.9 s for determining the pathloss for all 2356 measurement points of the three measurement routes.

IV. EVALUATION OF FEMTOPREDS' PREDICTIONS WITH POWER MEASUREMENTS

This section discusses the evaluation process of the FemtoPred at 2.1 GHz which is a common frequency band for LTE and 5G mobile radio communication in Germany. For previously recorded and georeferenced measurement data, a prediction is carried out with the FemtoPred. The measured and predicted power values are then compared.

In contrast to the previous validation section the frequency is higher, the utilized building data is more detailed and the comparison quantities are power values. Furthermore, the comparison takes place in a topology typical for mobile communications with TX locations above the building roofs. The power levels are measured in a retail mobile network using commercially available hardware and specified as part of the mobile radio communication standard LTE. The objective is to evaluate the prediction results of the FemtoPred for further frequency ranges based on self-measured power levels in the public mobile radio network.

A. MEASUREMENT OF RSS VALUES

The Ettus X310 Universal Software Radio Peripherals (USRPs) with TwinRX daughterboards were used to record the mobile radio frequency band. The recording setup is presented in [33] in a static environment. By supplying battery power in the trunk, the measurement equipment was used in a mobile configuration. An omnidirectional antenna (Panorama LGMDM4B-6-60-24-58) was mounted on the vehicle roof to minimize the influence from the vehicle bodyshell. For the exact localization of the measurements, a u-Blox C099-F9P application board was utilized, whose accuracy was processed with correction data via Real-time kinematic (RTK) and thus provides centimeter level accuracy. Configuration and communication with the USRPs was done via GnuRadio with UHD 4.2 driver running on an Ubuntu PC (AMD Ryzen Threadripper 2970WX, 256 GB RAM). During the measurements only IQ-samples were recorded, the data was processed afterwards using MathWorks MATLAB LTE-Toolbox. The measurement parameters were chosen so that a 100 ms sequence was recorded every half second, from which values such as RSRP, RSSI, RSRQ and PCI could be decoded. The recorded cellular radio samples and GNSS coordinates are matched via a unique time stamp. Depending on the cars' velocity the distance between two consecutive measurement sequences is about 3 m.

The TwinRX daughterboards record uncalibrated IQ samples that are scaled with respect to the receiver's analog-to-digital converter (ADC) voltage. Hence, they are related to a physical quantity by a certain factor and are represented in deciBel-Full Scale (dBF S). Decoded by the Mathworks MATLAB LTE-Toolbox, the IQ samples are used to compute the Reference Signal Received Power (RSRP) values, which gives a linear average of the power levels of the reference symbols (RS) distributed over the entire mobile radio frequency band and is therefore independent of the cell load. Those RSRP values enable a comparison to the predicted RSS values of the FemtoPred. With the values normalized with respect to the mean, the standard deviation functions as a comparison metric which works well under the assumption that the values are correctly predicted on average.

In total, 729 measured sequences were recorded and decoded in the 20 MHz downlink mobile radio frequency band of Telekom AG at 2.1 GHz. Each sequence decoded results in measurement samples. They reveal connections to 13 different mobile radio sectors. The measurement took place in urban and suburban areas and covers an area of approximately 13.5 km^2.

B. COMPARISON OF MEASUREMENT WITH RAY TRACING PREDICTIONS

The simulation is based on Level of Detail (LOD) 2 building data and exact cell site locations of the German mobile network operator (MNO) Deutsche Telekom AG. The FemtoPred is configured to search for direct, vertically and horizontally diffracted, scattered and up to the order of 2 reflected paths. Because all measurements have taken place outdoor and the attenuation by buildings is considered to be very high and the energy contribution therefore negligible, the calculation of propagation through buildings is omitted. The measured values are assigned to the mobile radio stations via the Physical Cell Identifier (PCI) on the one hand, but also via a precalculated Best Server Map (BSM) on the other. This is necessary because the PCI is not a unique identifier due to its limitation to 504 unique IDs. Some PCIs occur several times in the measurement area. Based on the assignment, the FemtoPred calculates a pathloss between the cell antenna location (TX) and the measurement position (RX). According to (1), this pathloss together with the transmit power and the antenna gain results in the RSS. For each individual cell, the mean value can thus be determined from the deviations between the associated, predicted RSS values and the measured RSRP values. Fig. 2 shows a histogram of RSS differences for all 729 measurement samples.

With a standard deviation of 9.5 dB, the differences between measured and predicted values are within the expected range. Differences arise from unmodeled environmental variations such as cars, bridges, underpasses, and vegetation. For example, shadowing from a passing metallic truck results in a leap of several dB in the measured power values. Since this is not modeled for the prediction, this leap is absent in the predicted values. Larger jumps in the predictions occur near the base station because neighboring measurement points lead to larger changes in the azimuth and elevation angle than measurement points further away from

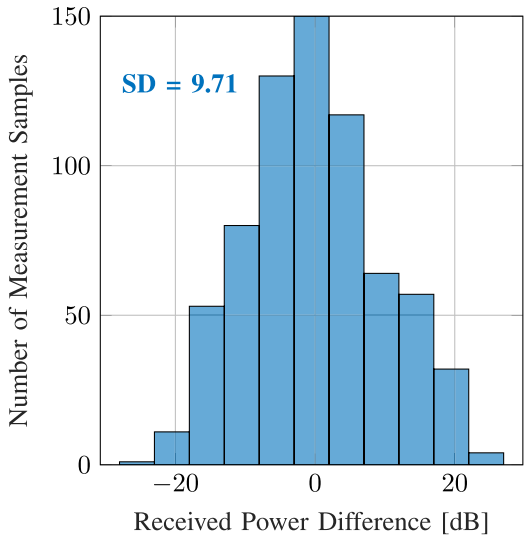

FIGURE 2. Histogram of differences in dB between measured and predicted normalized power levels.

the base station. Since these angular ranges are partly away from the main antenna beam direction, there are sometimes strong dips in the antenna pattern. In reality, such strong dips can only be measured in the laboratory.

V. INVESTIGATION OF MULTI PATH COMPONENTS WITH RAY TRACING IN A REAL WORLD SCENARIO

The simulations presented here take place in the urban area of the city of Braunschweig, Germany. Three dimensional building data from the municipality with LOD2 are utilized in combination with cell site locations of the MNO Deutsche Telekom AG. The ray tracing simulations are performed at a center frequency of 3600 MHz, the material parameters are taken from [16]. For the evaluation made here an isotropic antenna with 0 dBi is assumed. The FemtoPred is parameterized for this investigation as follows: Maximum reflection order of 2, diffraction over roofs and side walls, scattering, no transmission.

A. DISCUSSION OF RAY TRACING RESULTS

The FemtoPred calculates rays between two points within the scenario as introduced in Section II. Up to now one ray can only contain interactions of one type, i.e., a mixture between, e.g., a reflecting and a diffracted interaction in one ray is not possible. Fig. 3 illustrates the predicted RSS for one cell site location inside the city center of Braunschweig. The cell is located at a height of 29.16 m, the grid size is 5 m for a height of 1.5 m. The maximum distance between TX and RX is set to 2500 m which explains the circular shaped predictions. The green point in the middle of each figure depicts the cell site location. The color of each pixel indicates the absolute power each effect has for a particular map pixel in dBm. Gray pixels are either out of prediction range or inside buildings, since no transmission is considered.

The individual propagation effects greatly differ in terms of predicted coverage. Direct and reflected paths mostly exist in a small area around the base station, first-order reflection and direct paths predominantly at larger, unbuilt open areas. For second-order reflections fine structures like street canyons can be seen. Roof diffraction is by far the most common propagation type. A ray diffracted over roofs can always be found, except for those pixel for which a direct path is found. Side diffraction leads to a more ambiguous coverage pattern. It seems to be highly dependent on high profile buildings and is most pronounced in wide street canyons. The prediction of scattered rays shows a similar pattern, albeit more broadly spread but with less power.

The colors in Fig. 3 indicate the dominant power of direct and reflected paths when available. Naturally, the direct path is of course stronger than the reflected. In the open areas where both side diffraction and scattering occur, both effects slightly exhibit the same amount of power. The figure of the roof diffraction makes clear that for those pixels, where other propagation effects have been predicted, the roof diffraction plays only a minor role. In all other pixels the roof diffraction is the main propagation effect.

To get a more qualified impression of the spatial distribution of each effect on the map, Fig. 4 illustrates the occurrence probability and mean power of each effect as a function of distance. These results were gained by grouping samples into distance bins with a width of 5 m and computing the mean power and occurrence probability for each bin.

From Fig. 4 it can be seen that direct and reflected propagation occurs very rare above a distance of about 1100 m in this scenario. However, these rare rays have a high contribution to the pixels' RSS. Thus, deactivating ray tracing for reflection above a certain distance would partly lead to significant errors. Analyzing those distant map pixel, for which a direct or reflected propagation path was predicted, leads to the proposition that they are mostly located at unbuilt area, multiple meters away from buildings.

Also from the map in Fig. 3 areas could be identified where one propagation effect causes the main power contribution. Performing measurements at exactly those places allows to evaluate and possibly calibrate each propagation effect individually.

B. LOCATION BASED ACCELERATION TECHNIQUES

The observations of Fig. 4 match up with the findings of [35], [36], [37], [38], that the existence of rays with dedicated propagation mechanism is a function of the environment and the TX height in relation to the height of the surrounding buildings. Based on these observations, we derived a decision model for this type of scenarios with a TX height several meters above the surrounding roof tops. The model decides for each location on a map, whether to search for reflected rays. The distance to the TX as well as the height of the nearest building have a significant impact on the existence of this ray type. Let us therefore define three metrics to compute the distance to the nearest building for each RX location:

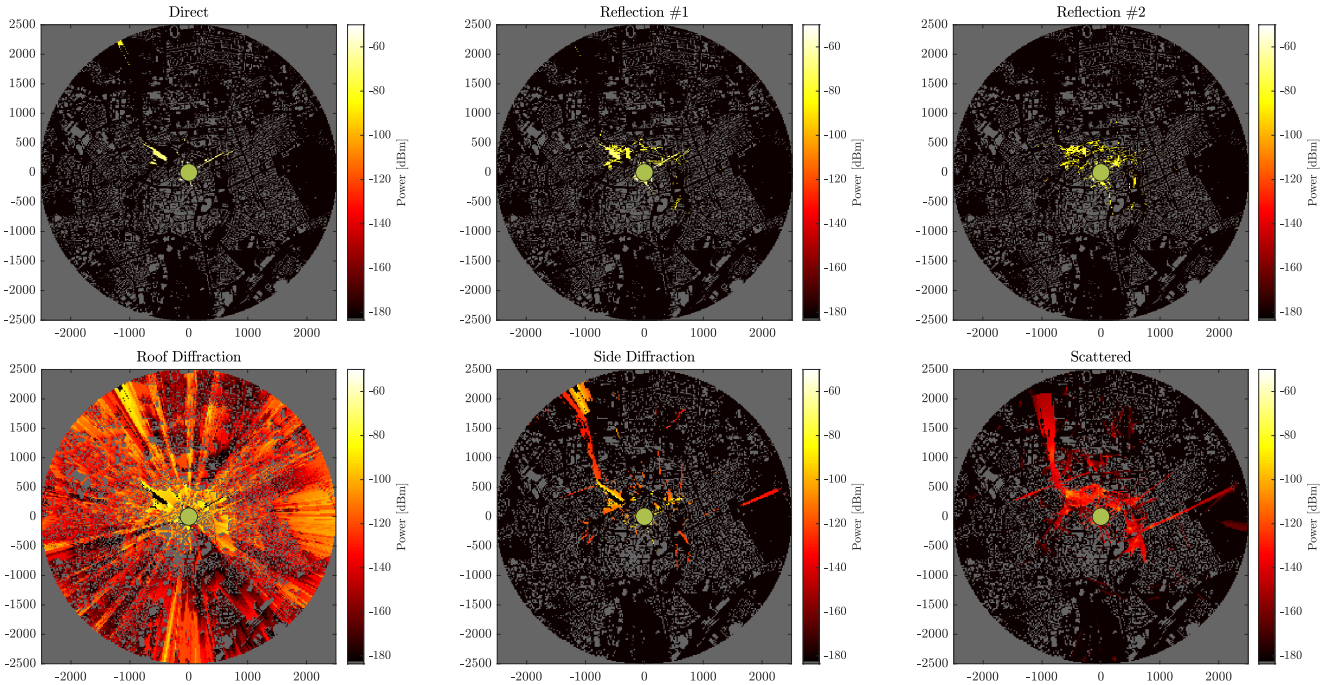

FIGURE 3. **Absolute power for each propagation effect individually. The green dot in the center indicates the cell site location. Grey pixels are either inside buildings or out of prediction range. The pixel raster size is 5 m.**

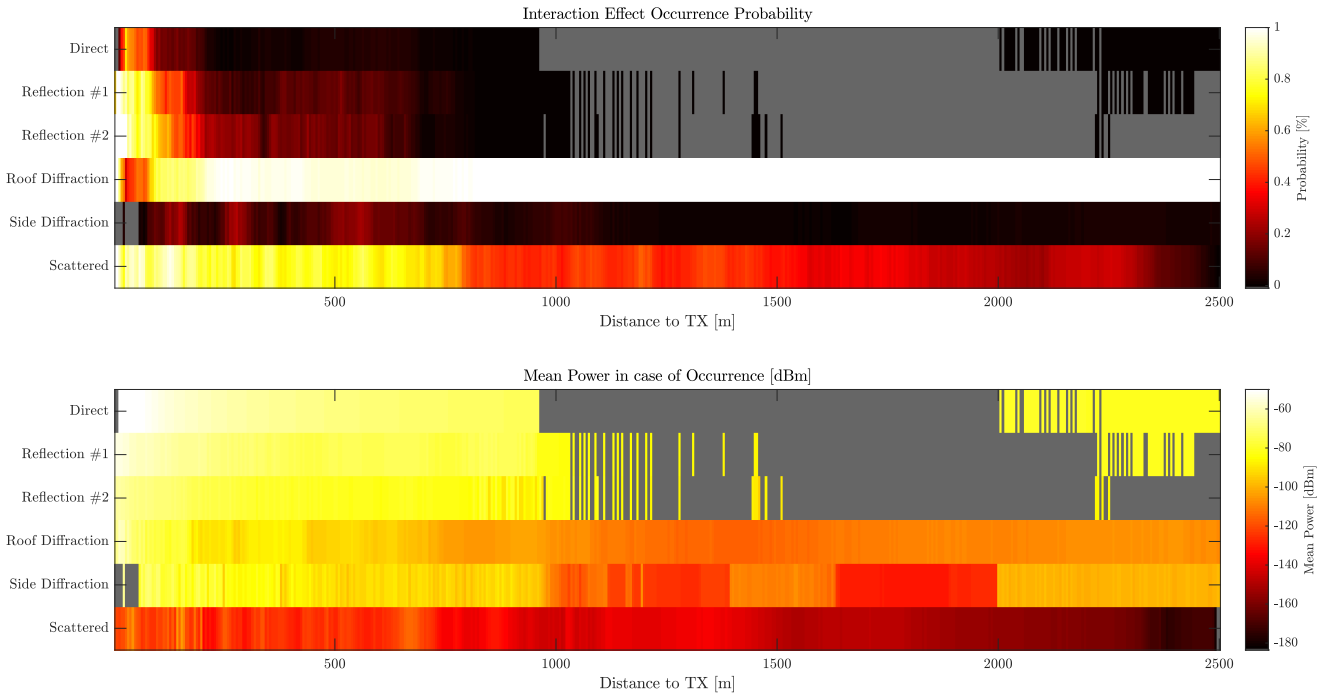

FIGURE 4. **Propagation effects as a function of distance between TX and RX.**

Method #1 determines the distance to the nearest building for each RX location.

Method #2, on the other hand, determines the distance to the nearest building in the direction of the base station.

Method #3 extends this by taking into account the building height. As mentioned above, reflected propagation paths are mostly located at unbuilt area. The heights of the surrounding buildings of this area clearly correlates with the distance from which the unbuilt area begins. To account for this, a correction term is added to the distance (dist) depending on the height of the building (z) following

$$\text{dist} = \begin{cases} \text{dist}, & \text{for } z \geq 10 \\ \text{dist} + 10 - z, & \text{for } z < 10. \end{cases}$$

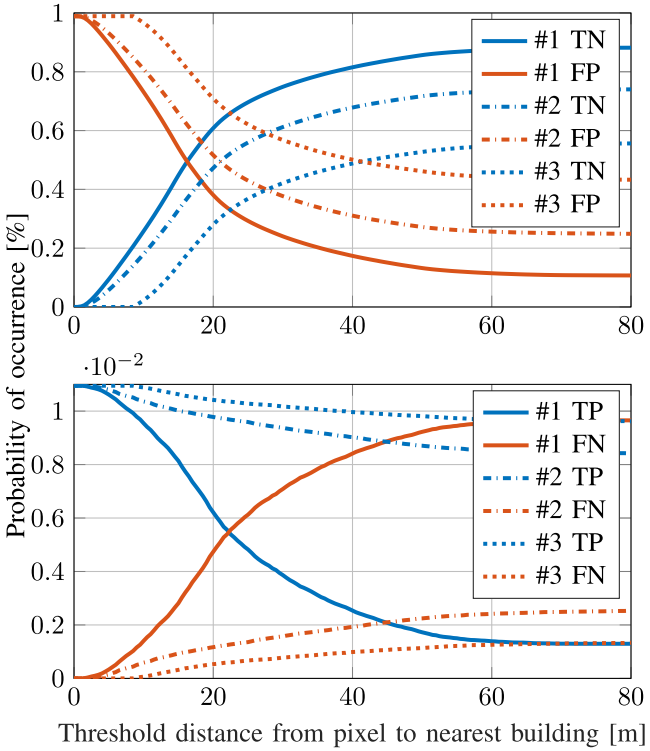

FIGURE 5. Filter performance as a function of threshold distance. Method #1 exhibits high False Negative (FN) values even at a short threshold distance which should be as low as possible in terms of accuracy. Method #2 performs better in terms of FN but has a lower True Negative (TN) rate which indicates a slightly lower acceleration.

Having all RX locations classified according to the models, a distance threshold can then be applied that determines whether a search for reflected paths should be performed for the respective RX location or not (in case the distance is lower than the threshold).

Fig. 5 presents the performance analysis of the acceleration approach for the three methods. There are 606769 map pixels to be predicted in the scenario. Among these, 6644 have a first order reflected path. The evaluation measures include True Positive (TP) pixels, classified as those with a distance higher than the threshold and exhibit reflected paths. False Positives (FP) are pixels that are also beyond the threshold but for which there are no reflected paths. For these pixels, a ray search for reflected paths is performed unnecessarily, so the number of FP pixels should be as low as possible. True Negative (TN) pixels, which are not considered for reflected ray search due to their proximity to buildings, should maximized to increase the effectiveness of this acceleration method. False Negative (FN) pixels are erroneously considered irrelevant due to their short distance to the nearest building, but actually exhibit reflected paths. Minimizing the number of FN pixels is crucial to reduce prediction inaccuracies introduced by this acceleration method.

The shape of the curves for Method #1 (continuous lines) shows strong shifts of the proportions already for low distance thresholds up to 30 m. The TN rate increases very fast and reaches already a value of approx. 60% for a distance of only 20 m. However, the FN rate increases similarly fast, which is why at this distance threshold already more than 45% of the actual pixels with reflected rays (i.e., 3769 pixels or 0,6% of all map pixels) are excluded from the ray search. The filtering of the map pixels based on their proximity to the nearest building turns out to be error-prone in this scenario, since already at a filtering of 20% of the pixels (Threshold distance = 8 m) about 9% of the relevant pixels are neglected (see FN rate).

For Method #2 (dash-dotted line), the proportions are different, in particular the FN curve is much flatter and even at a threshold distance of 80 m the FN rate is only 23% of the relevant pixels. At a threshold distance of 21 m, a reflection ray search has to be performed for only 50% of the map pixels. With filtering Method #2 and this threshold distance, false predictions occur for only 736 map pixels, i.e., 11% of the actual pixels with reflected rays.

Method #3 decreases the FN rate even further which leads to a more accurate result. This occurs at the expense of acceleration, as can be seen in the less-decreasing FP curve.

In order to investigate the generalization of the acceleration method, the three aforementioned methods were applied to additional 15 real 5G cell sites in the cities of Berlin, Braunschweig, Hanover and Wolfsburg. They have roughly the same height around 28 m and are located several meters above the building roof below. The total of 16 investigated cells are distributed over the entire city area and thus cover urban as well as suburban areas. For the comparability of the curves, the TN and FP values were normalized with the FP value for the threshold distance 0 m for each cell individually. The TP and FN values were normalized with the TP value for the threshold distance 0 m. Fig. 6 represents the mean and standard deviation for each of the three methods for all 16 cell sites.

From Fig. 6, a clear difference between the three methods presented is evident, both in the measure of acceleration (FP, lower is better) and in the error proneness (FN, lower is better). The magnitude of the standard deviation in FN values indicates the generalizability. Method #1 proves to be very error-prone, whereas Method #3 shows a very good generalizability. In contrast, the FP values indicate the acceleration gain, which can reach over 80% with Method #1. Method #3 achieves almost 45% from a distance threshold of 60 m.

Method #2 is in middle range between Method #1 and Method #3. The small deviation of the FN values for Method #2 and Method #3 in Fig. 5 is not apparent in Fig. 6, where it is significantly larger. The reason for this lies in the building heights. The cell that forms the basis for Fig. 3, Fig. 4, Fig. 5 is located in the urban area. Most of the remaining 15 cells also cover suburban areas that contain significantly flatter buildings. For these buildings, the simple distance consideration from Method #2 is more prone to error.

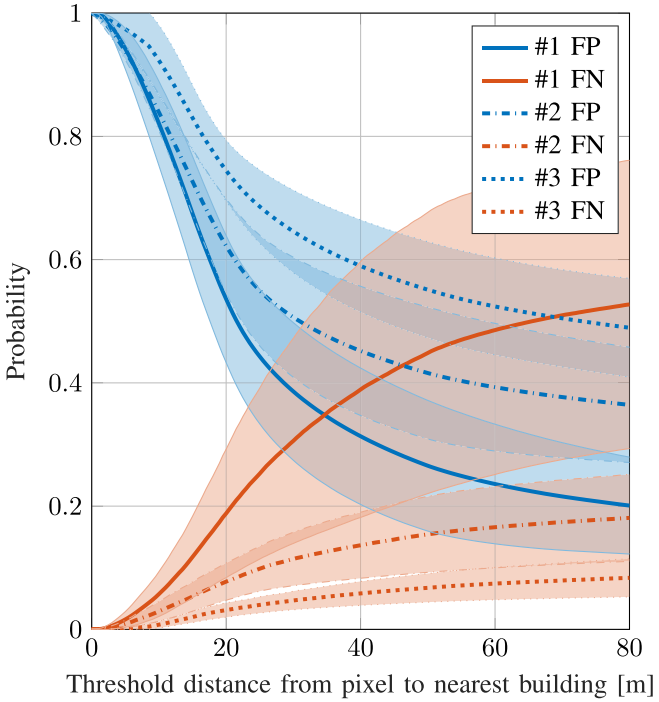

FIGURE 6. Overview of the generalization of the acceleration approach for the three methods presented. The mean value and the standard deviation for 16 mobile radio cells in the urban area are shown.

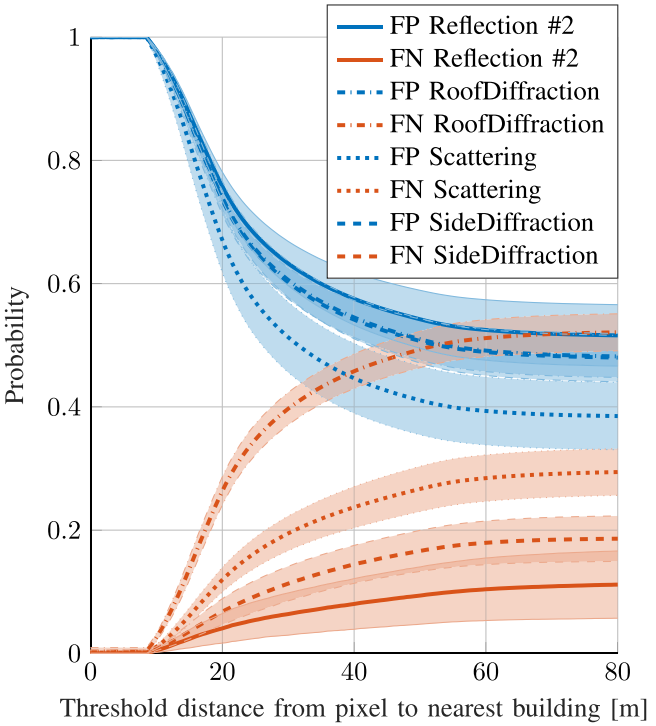

FIGURE 7. Method #3 applied for the remaining propagation effects.

Method #3 thus proves to be a significant acceleration option for reflected ray predictions of order 1, and the accompanying inaccuracy can be accepted, especially for map predictions over large areas. If more errors are tolerable or the prediction area contains only buildings with approximately the same height, Method #2 also provides a good acceleration possibility.

Applying the acceleration methods to the remaining propagation effects leads to mixed view. Fig. 7 visualizes the mean value and the standard deviation for the propagation effects reflection with order 2, roof diffraction, scattering and side diffraction. Since Method #3 yields to the lowest FN rate for all propagation effects, only those results are depicted in Fig. 7. It is shown in each case the FP and FN course.

From Fig. 7, it is clear that the acceleration method can be applied to the other propagation effects as well. However, the FN rates for roof diffraction and scattering are exceedingly high, which would lead to severe prediction errors. It is apparent from Fig. 3 that the distribution patterns of the pixels with the roof diffraction and scattering propagation effects are significantly different from those generated by the reflected paths. Thus, such a large prediction error is to be expected, which makes the acceleration approach for these effects not appropriate. Contrary, Method #3 can be used with reasonable error to determine side diffracted rays or second order reflected rays. The comparison between reflection order 1 (Fig. 6) and reflection order 2 (Fig. 7) shows a slightly worse performance of the method for reflection order 2, both in accuracy and acceleration.

The presented acceleration approach is thus primarily applicable to the search for reflected paths. Especially for large scenarios with many surfaces, such as urban scenarios, a reduction of the pixels for which a reflected path has to be searched by, for instance, 40% means an enormous speedup. For example the simulation for Fig. 3 took about 53 h whereof 19 % accounted for reflected rays. Saving 40 % of this time results in an acceleration gain of about 4 h. The acceleration approach is not designed for small city scenarios, other topologies like indoor or predictions, where accuracy is particularly important. Investigations of MicroCells with antenna height below the roof tops show fundamentally different characteristics in comparison to Fig. 3. Reflected paths only occur in the immediate proximity of the cell. For such a MicroCell scenario, the boundaries would be chosen smaller, resulting in a reduced number of surfaces and, thus, significantly reducing the computational effort. On the other hand, this allows for more detailed modeled scenarios and higher order propagation effects to be considered.

So far the introduced pixel classification is based on a single feature like the distance to the nearest building in the direction of TX (see Method #2 and #3). With the aid of the FemtoPred, ground truth training data could be generated for various scenarios, which could then be used to train a neural network for the pixel classification. This neural network could take into account a variety of parameters like other distance metrics (e.g., to behind buildings), material parameters of surrounding surfaces or degree of exposure. [34] presents a similar concept, but

here the complete prediction should happen with the help of neural networks. In the authors' opinion, the restriction to pixel classification has the advantage that the predictions are still deterministically based on the established models for the individual propagation effects, but they are accelerated enormously by the classification of the pixels.

Another possibility with this analysis method is to evaluate the different parameters of the distinguished propagation effects. For example, the reduction in the area into which surfaces are divided to determine scattering exhibit a saturating curve. If the size is further reduced, no significant differences in the result can be detected, but the calculation time increases drastically.

VI. CONCLUSION

This paper introduces the ray tracing algorithm called FemtoPred which is part of the SiMoNe framework. Necessary input data, ray search algorithms and implemented propagation models are listed and explained. To cope with the enormous computational complexity in big scenarios, FemtoPred includes methods and assumptions to accelerate predictions. The result format of FemtoPred enables for a detailed analyzing method of the individual propagation effects. Having sophisticated MPCs at hand allow among others for consideration of highly directive antennas or special network elements like IRS.

Validation of the FemtoPred is performed with the COST231 dataset which shows sufficient prediction quality of the algorithms. A subsequent evaluation with self-measured mobile radio power levels in the 2.1 GHz frequency range was able to confirm this finding. A comparison between measured and predicted power values in an urban environment shows a standard deviation of less than 10 dB.

From the detailed examination of the prediction results, an acceleration methodology for the search for dedicated propagation paths is derived. Our analyzing method facilitates to evaluate the significance of each MPC which is important for efficiency estimation of propagation prediction. It turns out that the acceleration method can be applied particularly well in predicting reflected paths. For an example scenario, a significant reduction in the number of pixels could be shown, for which a ray search for reflected paths must be performed. The resulting error is in the reasonable range depending on the intention of the prediction. Furthermore the detailed examination enables for a relative calibration process for each propagation effect individually. With a sufficient amount of measurement samples at dedicated positions, we are able to make a statement about how the pathloss predictions of the different propagation models fit to each other quantitatively.

The calibration of the ray tracer presented in this work was performed for the frequency at 2.1 GHz. It remains to be shown whether this prediction accuracy is also achieved for other mobile radio frequency bands. Furthermore, the studies presented so far have taken place in the urban and suburban area. The application of the proposed acceleration methods to rural areas and small scenarios like rooms or factory buildings is an interesting topic for further research activities.

REFERENCES

[1] M. Hata, "Empirical formula for propagation loss in land mobile radio services," *IEEE Trans. Veh. Technol.*, vol. 29, no. 3, pp. 317–325, Aug. 1980, doi: 10.1109/T-VT.1980.23859.

[2] N. Dreyer and T. Kürner, "A comparison of stochastic and deterministic channel models for V2V applications," in *Proc. Eur. Con. Netw. Commun. (EuCNC)*, 2020, pp. 79–83, doi: 10.1109/EuCNC48522.2020.9200903.

[3] C.-X. Wang, J. Huang, H. Wang, X. Gao, X. You, and Y. Hao, "6G wireless channel measurements and models: Trends and challenges," *IEEE Veh. Technol. Mag.*, vol. 15, no. 4, pp. 22–32, Dec. 2020, doi: 10.1109/MVT.2020.3018436.

[4] A. F. Molisch, "Deterministic channel-modeling methods," in *Wireless Communications*, 2nd ed. Chichester, U.K.: Wiley, 2011.

[5] A. F. Molisch, "Propagation Mechanisms," in *Wireless Communications*, 2nd ed. Chichester, U.K.: Wiley, 2011.

[6] C. A. Balanis, "Radiation integrals and auxiliary potential functions," in *Antenna Theory: Analysis and Design*, 3rd ed. Hoboken, NJ, USA: Wiley, 2016.

[7] D. M. Rose, T. Jansen, T. Werthmann, U. Turke, and T. Kurner, "The urban hannover scenario - realistic 3D pathloss predictions and mobility patterns," in *Proc. IEEE 84th Veh. Technol. Conf. (VTC-Fall)*, 2016, pp. 1–7, doi: 10.1109/VTCFall.2016.7881253.

[8] D. M. Rose, J. Baumgarten, S. Hahn, and T. Kurner, "SiMoNe - Simulator for mobile networks: System-level simulations in the context of realistic scenarios," in *Proc. IEEE 81st Veh. Technol. Conf. (VTC Spring)*, 2015, pp. 1–7, doi: 10.1109/10.1109/VTCSpring.2015.7146084.

[9] J. M. Eckhardt, C. Herold, B. K. Jung, N. Dreyer, and T. Kürner, "Modular link level simulator for the physical layer of beyond 5G wireless communication systems," *Radio Sci.*, vol. 57, no. 2, pp. 1–15, Feb. 2022, doi: 10.1029/2021RS007395.

[10] F. A. Agelet, A. Formella, J. M. H. Rabanos, F. Isasi de Vicente, and F. P. Fontan, "Efficient ray-tracing acceleration techniques for radio propagation modeling," *IEEE Trans. Veh. Technol.*, vol. 49, no. 6, pp. 2089–2104, Nov. 2000, doi: 10.1109/25.901880.

[11] W. Hunt and W. R. Mark, "Ray-specialized acceleration structures for ray tracing," in *Proc. IEEE Symp. Interact. Ray Tracing*, Los Angeles, CA, USA, 2008, pp. 3–10, doi: 10.1109/RT.2008.4634613.

[12] Y. Deng, Y. Ni, Z. Li, S. Mu, and W. Zhang, "Toward real-time ray tracing: A survey on hardware acceleration and microarchitecture techniques," *ACM Comput. Surv.*, vol. 50, no. 4, pp. 1–41, Jul. 2018, doi: 10.1145/3104067.

[13] T. Kürner and A. Meier, "Prediction of outdoor and outdoor-to-indoor coverage in urban areas at 1.8 GHz," *IEEE J. Sel. Areas Commun.*, vol. 20, no. 3, pp. 496–506, Apr. 2002, doi: 10.1109/49.995508.

[14] N. Dreyer and T. Kürner, "An analytical raytracer for efficient D2D path loss predictions," in *Proc. 13th Eur. Conf. Antennas Propag. (EuCAP)*, Krakow, Poland, 2019, pp. 1–5.

[15] F. Sheikh et al., "THz measurements, antennas, and simulations: From the past to the future," *IEEE J. Microw.*, vol. 3, no. 1, pp. 289–304, Jan. 2023, doi: 10.1109/JMW.2022.3216210.

[16] *Effects of Building Materials and Structures on Radiowave Propagation Above About 100 MHz*, ITU-Rec. P. 2040, Int. Telecommun. Union, Geneva, Switzerland, 2021.

[17] *Propagation Data and Prediction Methods for the Planning of Short-Range Outdoor Radiocommunication Systems and Radio Local Area Networks in the Frequency Range 300 MHz to 100 GHz*, ITU-Rec. P. 1411-11, Int. Telecommun. Union, Geneva, Switzerland, 2021.

[18] *Propagation Data and Prediction Methods for the Planning of Indoor Radiocommunication Systems and Radio Local Area Networks in the Frequency Range 900 MHz to 100 GHz*, ITU-Rec. P. 1238-7, Int. Telecommun. Union, Geneva, Switzerland, 2012.

[19] J. Deygout, "Correction factor for multiple knife-edge diffraction," *IEEE Trans. Antennas Propag.*, vol. 39, no. 8, pp. 1256–1258, Aug. 1991, doi: 10.1109/8.97368.

[20] M. Born and E. Wolf, *Principles of Optics: 60th Anniversary Edition*, 7th ed. Cambridge, U.K.: Cambridge Univ., 2019. [Online]. Available: http://dx.doi.org/10.1017/9781108769914
[21] T. G. Mackay and A. Lakhtakia, *The Transfer-Matrix Method in Electromagnetics and Optics*. Cham, Switzerland: Springer, 2022.
[22] J. G. Meana, J. Á. Martinez-Lorenzo, F. Las-Heras, and C. Rappaport, "Wave scattering by dielectric and lossy materials using the modified equivalent current approximation (MECA)," *IEEE Trans. Antennas Propag.*, vol. 58, no. 11, pp. 3757–3761, Nov. 2010, doi: 10.1109/TAP.2010.2071363.
[23] S. M. Rubin and T. Whitted, "A 3-dimensional representation for fast rendering of complex scenes," in *Proc. 7th Annu. Conf. Comput. Graph. Interact. Techn.*, 1980, pp. 110–116, doi: 10.1145/965105.807479.
[24] G. Wolfle, B. E. Gschwendtner, and F. M. Landstorfer, "Intelligent ray tracing-a new approach for field strength prediction in microcells," in *Proc. IEEE 47th Veh. Technol. Conf. Technol. Motion*, Phoenix, AZ, USA, 1997, pp. 790–794, doi: 10.1109/VETEC.1997.600437.
[25] V. Degli-Esposti, F. Fuschini, and M. Amorini, "Database simplification for field prediction in urban environment [radiowave propagation]," in *Proc. IEEE Antennas Propag. Soc. Symp.*, Monterey, CA, USA, 2004, pp. 1619–1622, doi: 10.1109/APS.2004.1330503.
[26] A. Guttman, "R-trees: A dynamic index structure for spatial searching," in *Proc. ACM SIGMOD Int. Conf. Manag. Data (SIGMOD)*, New York, NY, USA, 1984, pp. 47–57, doi: 10.1145/602259.602266.
[27] "COST 231 Munich digital map and measurements." Accessed: Sep. 5, 2023. [Online]. Available: https://propagationtools.com/wireless/cost-231-munich-digital-map-and-measurements/
[28] *Directorate-General for the Information Society and Media: Propagation Prediction Models: COST Action 231: Digital Mobile Radio Towards Future Generation Systems: Final Report*, Eur. Comm., Brussels, Belgium, 1999.
[29] Z. Yun, Z. Zhang, and M. F. Iskander, "A ray-tracing method based on the triangular grid approach and application to propagation prediction in urban environments," *IEEE Trans. Antennas Propag.*, vol. 50, no. 5, pp. 750–758, May 2002, doi: 10.1109/TAP.2002.1011243.
[30] Z. Lai, N. Bessis, G. de Laroche, H. Song, J. Zhang, and G. Clapworthy, "An Intelligent ray launching for urban prediction," in *Proc. 3rd Eur. Conf. Antennas Propag.*, Berlin, Germany, 2009, pp. 2867–2871.
[31] S. Hussain and C. Brennan, "An image visibility based pre-processing method for fast ray tracing in urban environments," in *Proc. 10th Eur. Conf. Antennas Propag. (EuCAP)*, Davos, Switzerland, 2016, pp. 1–5, doi: 10.1109/EuCAP.2016.7481422.
[32] T. Alwajeeh, P. Combeau, and L. Aveneau, "An efficient ray-tracing based model dedicated to wireless sensor network simulators for smart cities environments," *IEEE Access*, vol. 8, pp. 206528–206547, 2020, doi: 10.1109/ACCESS.2020.3037135.
[33] N. Spicher, M. Schweins, L. Thielecke, T. Kürner, and T. M. Deserno, "Feasibility analysis of fifth-generation (5G) mobile networks for transmission of medical imaging data," in *Proc. 43rd Annu. Int. Conf. IEEE Eng. Med. Biol. Soc. (EMBC)*, Mexico, 2021, pp. 1791–1795, doi: 10.1109/EMBC46164.2021.9629615.
[34] M. Sasaki et al., "Multi-input RNN based proactive prediction of path loss using building information in UMa environments," *IEICE Tech. Rep.*, vol. 122, no. 339, pp. 18–23, 2023. [Online]. Available: https://ken.ieice.org/ken/paper/20230119rCQD/eng/
[35] S. Hussain, D. Trinh, and C. Brennan, "Mixed path loss model for urban environments," in *Proc. 9th Eur. Conf. Antennas Propag. (EuCAP)*, Lisbon, Portugal, 2015, pp. 1–5.
[36] N. J. Thomas, M. J. Willis, and K. H. Craig, "The relative importance of different propagation mechanisms for radio coverage and interference prediction in urban scenarios at 2.4, 5.8, and 28 GHz," *IEEE Trans. Antennas Propag.*, vol. 54, no. 12, pp. 3918–3920, Dec. 2006, doi: 10.1109/TAP.2006.886571.
[37] S. Y. Tan, "Investigation of propagation mechanisms in a typical cellular communication system," in *Proc. Asia-Pacific Microw. Conf. Proc. (Cat. No.00TH8522)*, Sydney, NSW, Australia, 2000, pp. 253–256, doi: 10.1109/APMC.2000.925778.
[38] H. Miao et al., "Sub-6 GHz to mmWave for 5G-advanced and beyond: Channel measurements, characteristics and impact on system performance," *IEEE J. Sel. Areas Commun.*, vol. 41, no. 6, pp. 1945–1960, Jun. 2023, doi: 10.1109/JSAC.2023.3274175.

MICHAEL SCHWEINS received the M.Sc. degree in electrical engineering from Technische Universität Braunschweig, Germany, in 2017, where he is currently pursuing the Ph.D. degree with the Department of Mobile Radio Systems, Institute for Communications Technology. His research interests include mobile radio channel predictions, system-level simulations, and advanced antenna technology.

LENNART THIELECKE received the M.Sc. degree in electrical engineering from the Technische Universtität Braunschweig, Germany, in 2018, where he is currently pursuing the Ph.D. degree wit the Department of Mobile Radio Systems, Institute for Communications Technology. His research interests include SDR-based measurement solutions, real-time channel emulation and vehicular communications.

NILS GRUPE received the M.Sc. degree in electrical engineering and the Dr.-Ing. degree from Technische Universität Braunschweig, Germany, in 2014 and 2023, respectively, where he worked as a Researcher with the Department of Mobile Radio Systems, Institute for Communications Technology from 2015 to 2021. His main research was on new accelerating techniques to speed up ray optical path loss predictions. He further worked on new simulation concepts to model realistic V2X communication scenarios. Since 2022, he has been working at mission critical broadband communications with the Innovations Department, HMF Smart Solutions GmbH.

THOMAS KÜRNER (Fellow, IEEE) received the first Dipl.-Ing. degree in electrical engineering and the second Dr.-Ing. degree from the University of Karlsruhe, Germany, in 1990 and 1993, respectively. From 1990 to 1994, he was with the Institut für Höchstfrequenztechnik und Elektronik, University of Karlsruhe, working on wave propagation modeling, radio channel characterization and radio network planning. From 1994 to 2003, he was with the Radio Network Planning Department at the headquarters of the GSM 1800 and UMTS operator E-Plus Mobilfunk GmbH & Co KG, Düsseldorf, where he was a team manager radio network planning support. Since 2003, he has been a Full University Professor of Mobile Radio Systems with Technische Universität Braunschweig. He was the Project Coordinator of the H2020-EU-Japan Project ThoR ("TeraHertz end-to-end wireless systems supporting ultra-high data Rate applications") and is a Coordinator of the German DFG-Research Unit FOR 2863 Meteracom ("Metrology for THz Communications"). He is currently chairing the IEEE 802.15 Standing Committee THz and the ETSI Industrial Specification Group THz. He was also the Chair of IEEE 802.15.3d TG 100G.